CrystEngComm

PAPER

View Article Online
View Journal | View Issue

Cite this: *CrystEngComm*, 2025, **27**, 1026

Salt formation of cabozantinib with hydrochloric and hydrobromic acids – influence on the *in vitro* dissolution behavior and food effect†

Sreela Ramesh,[ac] Eliška Zmeškalová,[ab] Monika Kučeráková,[b] Vít Zvoníček[c] and Miroslav Šoóš *[a]

Received 18th December 2024,
Accepted 20th December 2024

DOI: 10.1039/d4ce01278j

rsc.li/crystengcomm

The aim of this study was to prepare stable novel crystalline salts of cabozantinib, a tyrosine kinase inhibitor used to treat medullary thyroid cancer, to improve its dissolution properties and thereby reduce the positive food effect associated with its marketed salt form (L-malate). Five novel multi-component solid forms were obtained. In addition to the detailed physicochemical characterization, we report the crystal structures of the saccharinate, hydrochloride, and hydrobromide salts. The hydrobromide and hydrochloride salts of cabozantinib were chosen for further studies based on promising preliminary results from dissolution rate measurements. The potential of the hydrochloride and hydrobromide salts to be used for drug formulation was determined by testing their physical stability using hygroscopicity tests and by observing their melting properties. To investigate the impact of these salts on reducing the patient-relevant food effect, *in vitro* dissolution studies in stimulated fed and fasted states using biorelevant media were performed and compared to the marketed form of the drug.

1. Introduction

New molecular entities (NMEs) today are frequently large-molecular-weight, lipophilic, and poorly water-soluble compounds that most often fall into BCS Class II.[1] BCS class II drugs characterized by low solubility and high permeability have a tendency to display a positive food effect (increased solubility in the fed state) associated with them.[2] The U.S. FDA issued a guidance in December 2002 entitled "Food-Effect Bioavailability and Fed Bioequivalence Studies".[3] High-fat meal studies are recommended by the FDA, since such meal conditions are expected to provide the greatest effects on gastrointestinal physiology so that systemic drug availability is maximally affected. The common belief is that food effects result from changes in drug solubility and other factors as listed by the FDA that food may: "delay gastric emptying; stimulate bile flow; change the gastrointestinal pH; increase splanchnic blood flow; change the luminal metabolism of a drug substance, and physically or chemically interact with a dosage form or a drug substance."

Cabozantinib, a BCS class II drug, is a small-molecule multi-target tyrosine kinase inhibitor (smTKI).[4] The U.S. Food and Drug Administration has approved cabozantinib to be used in the treatment of renal cell carcinoma and progressive metastatic medullary thyroid cancer.[5] Cabozantinib is marketed under the trade names Cabometyx and Cometriq[6,7] in the form of tablets and capsules, respectively. It is marketed in the form of a salt with L-malic acid in both formulations.[8] Cabozantinib is found to have a positive food effect associated with it, and hence, it is not advised to be taken along with food.[9] smTKIs like cabozantinib have low solubility *in vivo*, which limits absorption and hence gives way to undesirable pharmacokinetic changes in the presence of food.[10] Clinically, such food–drug interactions for smTKIs are predicted to occur due to metabolism by cytochrome P-450 isoenzymes hepatically.[11] The critical importance of thoroughly investigating the influence of food on the bioavailability of these drugs cannot be overstated and such insights must be explicitly addressed in the labeling of these marketed drugs to ensure that patients and healthcare providers have the necessary guidance for appropriate administration.[12] A recent report[13] shows how oral absorption of cabozantinib was improved approximately 2-fold in rats by converting it to a lipid-based formulation containing its docusate salt. Since the absorption of cabozantinib is limited by its solubility, discovering new formulations that can dissolve

[a] *Department of Chemical Engineering, University of Chemistry and Technology, Technická 3, 166 28 Prague 6 – Dejvice, Czech Republic.*
E-mail: miroslav.soos@vscht.cz
[b] *Department of Structure Analysis, Institute of Physics of the Czech Academy of Sciences, Na Slovance 1999/2, 182 00 Praha 8, Czech Republic*
[c] *Zentiva, k.s, U Kabelovny 130, 10237 Prague 10, Czech Republic*

† Electronic supplementary information (ESI) available: Solution ^{1}H NMR spectra, additional XRPD patterns, additional crystallographic data, IDR curves from experimental data and DSC curves, CCDC: 2303273, 2303274 and 2347514. For ESI and crystallographic data in CIF or other electronic format see DOI: https://doi.org/10.1039/d4ce01278j

Table 1 pK_a of the acids forming novel salts of cabozantinib

Acid	pK_a
Saccharin	1.6
Cyclamic acid	1.71
Tartaric acid	2.72
Hydrochloric acid	−6
Hydrobromic acid	−9

better can possibly help eliminate the food effect associated with the drug.

One of the best and easiest ways to improve the solubility of ionizable drugs is through salt formation.[14] For instance, by sulfonate salt formation, up to 200-times faster dissolution of an antidepressant agomelatine was achieved.[15] A previous study conducted by our group to improve the dissolution properties of an anti-psychotic drug cyamemazine showed how salt formation with dicarboxylic acids helped achieve better solubility.[16] In a study conducted by Mannava *et al.*, a 25-fold increase in the dissolution properties and subsequent enhancement of the bioavailability of the antituberculosis drug ethionamide was obtained by salt formation with oxalic acid.[17]

The basic nitrogen of cabozantinib has a pK_a of 5.9,[18] and hence for salt formation, the acid should have a pK_a value such that the pK_a difference between the API and the salt-forming co-former is 3 or more.[19] After an initial round of extensive screening, salts were formed with tartaric acid, cyclamic acid, saccharin, hydrobromic acid, and hydrochloric acid. The pK_a values of these acids[20–22] are listed in Table 1 and were found to be in agreement with the general delta pK_a ≥ 3 rule. The preparation and preliminary analysis (X-ray powder diffraction (XRPD) patterns and solution ^{1}H nuclear magnetic resonance (NMR) spectra) of these salts are described in detail in the coming sections. The crystal structures of the saccharinate, hydrochloride, and hydrobromide salts were solved from single-crystal X-ray diffraction. *In vitro* dissolution measurements allowed for the identification of the best candidates (hydrochloride and hydrobromide salts) to undergo thermal analysis and hygroscopicity tests. Finally, the capability of hydrobromide and hydrochloride salts to reduce the interaction with food was studied by *in vitro* dissolution tests in biorelevant media.

2. Experimental

2.1 Materials

Cabozantinib (CBZ) was kindly provided by Zentiva, k.s. solvents and acids of analytical purity were obtained from various commercial suppliers and were used as received.

2.2 Solution-mediated salt preparation

CBZ (20 mg) and the acids (tartaric acid, saccharin, cyclamic acid, hydrochloric acid and hydrobromic acid) were added in a 1 : 1 molar ratio in 500 μL of acetone into glass vials. Salt formation happened through slurry conversion, and the contents of the vial were filtered through a laboratory glass funnel (frit S3) under a vacuum. The filtered powders were dried in a vacuum oven at 40 °C. The CBZ L-malate salt was prepared by the evaporation method. CBZ (20 mg) and L-malic acid were added in a 1 : 1 ratio to 500 μL of tetrahydrofuran (THF) into a glass vial and heated until completely dissolved. The vial was left in the hood for the solvent to evaporate leaving behind the crystalline salt. The salt was dried overnight in a vacuum oven at 35 °C.

2.3 Single-crystal preparation

Single crystals of CBZ·HCl, CBZ·HBr and CBZ saccharinate salts were obtained by dissolving 2 mg of the salts in 150 μL of methanol, 150 μL of ethanol and a mixture of 100 μL of methanol and 100 μL of ethanol, respectively, in 1.5 ml glass vials. The lids were perforated with a needle to allow very slow solvent evaporation, resulting in single crystals.

2.4 Analytical methods

2.4.1 X-ray powder diffraction. The X-ray powder diffraction (XRPD) patterns were obtained using a powder diffractometer X'PERT PRO MPD PANalytical; X-ray beam Cu Kα (λ = 1.542 Å), excitation voltage: 45 kV, anodic current: 40 mA, measured range: 2–40° 2Θ, and step size: 0.01° 2Θ, remaining at a step for 0.05 s. The measurement was performed on a flat sample of area/thickness 10/0.5 mm. 0.02 rad Soller slits, a 10 mm mask, and 1/4° fixed anti-scattering slits were used to correct the primary beam. The irradiated area of the sample was 10 mm^2; programmable divergent slits were used. 0.02 rad Soller slits and 5.0 mm anti-scattering slits were used to correct the secondary beam.

2.4.2 Single crystal X-ray diffraction. The analysis was performed at 95 K for CBZ·HCl and CBZ·HBr salts using a SuperNova diffractometer with a micro-focus sealed tube, mirror-collimated Cu Kα radiation (λ = 1.54184 Å), and a CCD detector Atlas S2. The CBZ saccharinate salt was analyzed at 140 K X-ray on an Xcalibur, Gemini ultra diffractometer using the Cu-Kα radiation (λ = 1.5418 Å) from a fine-focus sealed X-ray tube with a graphite monochromator and a CCD detector Atlas S2. The data reduction and absorption correction were done using CrysAlisPro software[23] The structures were solved by charge flipping methods using Superflip software and refined by full-matrix least squares on the F^2 value using Crystals and Jana2006 (ref. 24 and 25) software. MCE software was used for the visualization of residual electron density maps.[26] The structures were deposited into the Cambridge Structural Database under numbers 2303273, 2303274 and 2347514.

2.4.3 Differential scanning calorimetry. Differential scanning calorimetry (DSC) measurements were performed on the TA Instruments Discovery DSC. The sample was weighed in an aluminum pan (40 μL), covered, and measured in the flow of a nitrogen gas. The investigation was performed in the temperature range from 0 to 300 °C at a heating rate of 5 °C min^{-1} (amplitude = 0.8 °C; period = 60 s). The peak maximum temperature (T_{peak}) was specified in the DSC result. The

enthalpy was given in the unit J g^{-1}. The sample weight was about 3–5 mg.

2.4.4 Thermogravimetric analysis. Thermogravimetric analysis (TGA) was performed on a TG 209, Netzsch instrument. Approximately 20 mg of the sample was weighed into a ceramic pan and measured under a nitrogen atmosphere. The TGA measurement was performed in the approximate temperature range 20–300 °C. A heating rate of 10 °C min^{-1} was used in all experiments.

2.4.5 Dynamic vapor sorption. Gravimetric moisture sorption analysis was carried out using a humidity and temperature controlled microbalance dynamic vapor sorption (DVS) apparatus, DVS Advantage 1 (Surface Measurement Systems, U.K.), with a Cahn D200 recording ultra-microbalance with a mass resolution of ±0.1 μg. Samples of approximately 20 mg were dried at 0% relative humidity (RH) under a nitrogen stream at 25 °C. The moisture uptake (reported relative to the dry weight) was monitored over a sorption/desorption range of 0–90% RH in increments of 10%.

2.4.6 Intrinsic dissolution rate. The intrinsic dissolution rate (IDR) was determined *via* a Sirius inForm (Pion Inc., USA) device to characterize the dissolution properties of the used substances. IDR discs with a 3 mm diameter were prepared by the compression of 20–30 mg of the material using a 100 kg weight equivalent, relaxed for one minute, and compressed again at a constant load of 100 kg for a second minute. IDR measurements at neutral pH (pH 6.8) were performed using 50 mL of phosphate buffer solution with 0.1% SDS at 100 rpm. For analyses in biorelevant media (fed state simulated intestinal fluid (FeSSIF) and fasted state simulated intestinal fluid (FaSSIF)), IDR measurements were performed using 50 mL of the respective buffer at 100 rpm. UV spectra were recorded every 30 s, and the optical path length was 20 mm. Even though the lambda max of

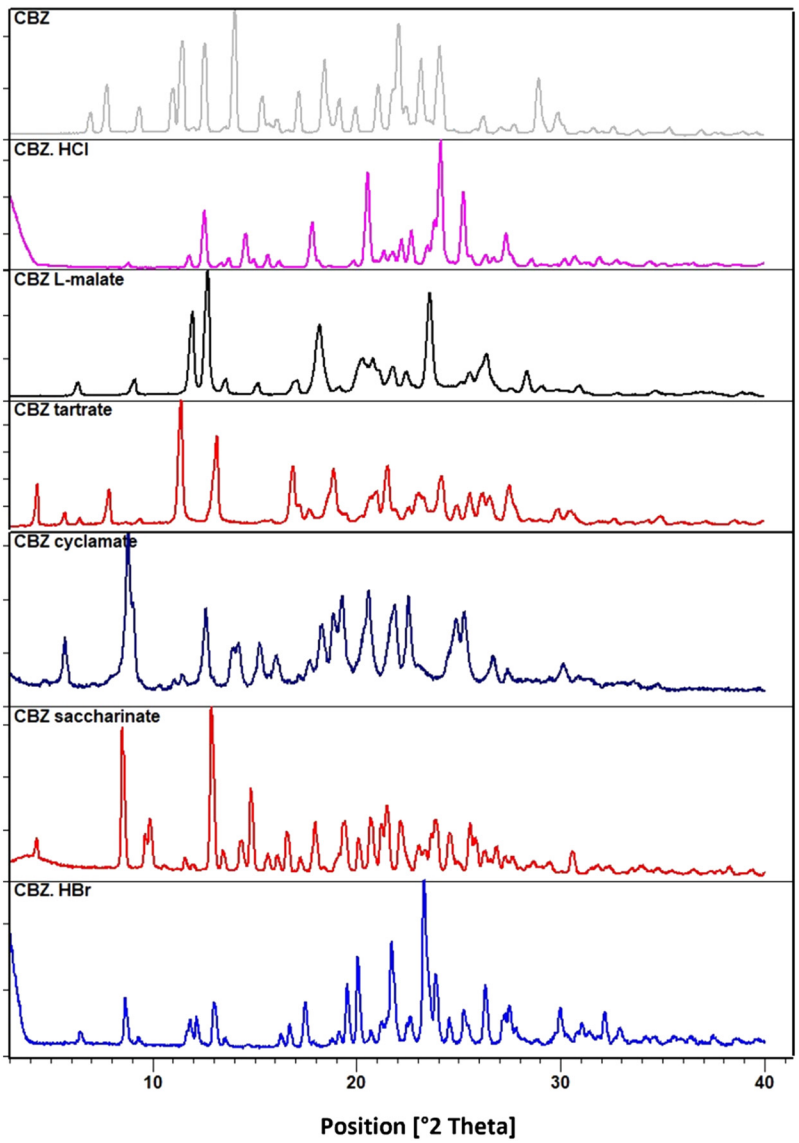

Fig. 1 XRPD patterns of the salts with cabozantinib.

cabozantinib was found to lie between 200 and 250 nm, absorption was too high and not within the acceptable range. Hence, absorbance between wavelengths of 300 nm and 400 nm was used to evaluate the amount of released API at each time point. The IDR was calculated using a zero-order linear fit through the experimental data. All measurements were performed in triplicate.

3. Results and discussion

3.1 Crystalline salts of CBZ

Solid forms obtained with saccharin, cyclamic acid, tartaric acid, hydrochloric acid and hydrobromic acid using the methods described in section 2.2 were characterized using XRPD analysis (Fig. 1). All forms were found to be novel crystalline solids as their XRD patterns were different from those of the starting materials. Even though CBZ·HBr, CBZ·HCl and CBZ saccharinate were confirmed to be salts from their crystal structure data, single crystals of CBZ tartrate and CBZ cyclamate could not be obtained. But, the IR spectra (Fig. S1†) of these compounds reveal a characteristic broad stretch in the region 2300 to 2700 cm^{-1}, indicative of protonation of the basic tertiary nitrogen in cabozantinib since absorption in this area in IR spectroscopy is associated with the NH^+ stretch. Moreover, a lack of absorption in this area for pure cabozantinib even further confirms protonation in the salts. Solution ^1H NMR (Fig. S2†) suggested that the salts with cyclamic acid, saccharin, and tartaric acid were indeed 1:1 salts. Due to the broadness of the peaks, this could not be determined for the CBZ·HCl and CBZ·HBr salts from solution NMR data, but their solved crystal structures prove the ratio to be also1 : 1. The CBZ L-malate salt prepared according to the method in section 2.2 was analyzed using XRPD (Fig. S3†) and used as a reference for the marketed form of the drug for dissolution studies.

3.2 Preliminary intrinsic dissolution rate measurement

Since the study's main aim was to find solid forms with higher dissolution rates than the marketed L-malate salt, the IDRs (Fig. 2) of all the salts were measured. The rates were measured at a neutral pH of 6.8 in phosphate buffer with 0.1% SDS to mimic the pH range of the fasted state of the human small intestine. CBZ saccharinate and CBZ tartrate salts dissolved slower than the CBZ L-malate salt, whereas the CBZ cyclamate salt had a slightly higher rate compared to the CBZ L-malate salt. CBZ·HBr and CBZ·HCl salts were found to dissolve at least two times faster than the marketed CBZ L-malate salt.

The significantly faster dissolution of CBZ·HCl and CB·HBr compared to other salts maybe attributed to the high strength of these acids, which in turn implies a high ionizing power and dissociation. The solubility of the drug cations in aqueous environments is hence higher contributing to faster dissolution. The smaller anion sizes for Cl^- and Br^- compared to the organic, larger anions like tartrate or saccharinate also probably allows for simpler packing of the salts and higher hydration energies aiding improved solubility.

3.3 Crystal structures

To get an insight into the crystal packing and interactions of CBZ with the counterions, we attempted to prepare their single crystals and solve their structures. We were successful in the preparation of the CBZ·HCl, CBZ·HBr and CBZ saccharinate salts. The data confirmed the protonation of the aromatic quinoline nitrogen of cabozantinib and, therefore, confirmed that these solid forms are salts and not co-crystals. The selected structural parameters are shown in Table 2. All other details about the measurement and refinement, as well as the geometry and H-bonding tables, can be found in the ESI† (Tables S1 and S2). The figures depicting the asymmetric unit with the thermal ellipsoids, the unit cell with highlighted anions, and H-bonding patterns are shown in Fig. 3.

CBZ·HCl crystallizes in the monoclinic system in the space group $P2_1/c$. There is one molecule of the CBZ cation and one chloride anion in the asymmetric unit and four of each in the unit cell, thus confirming the 1 : 1 ratio. The H-bonds run along the *b* direction, making an infinite chain of –CBZ–Cl–CBZ–, connected by quinoline N(3)H···Cl^-···HN(2) amidic H-bonds. In addition, there is also an intramolecular

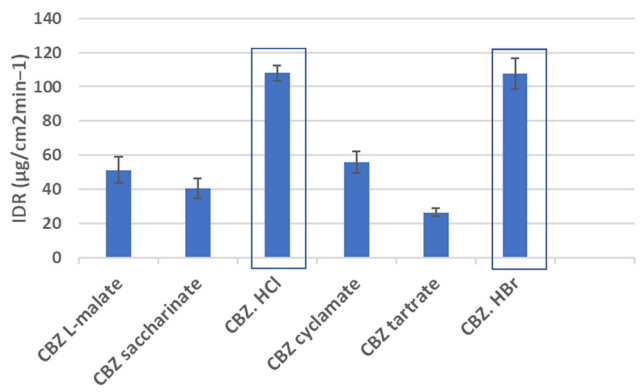

Fig. 2 IDR for the salts of CBZ at a pH of 6.8.

Table 2 Crystallographic data of structures of the salts of CBZ

	CBZ·HCl	CBZ·HBr	CBZ saccharinate
Formula	$C_{28}H_{25}Cl_1F_1N_3O_5$	$C_{28}H_{25}Br_1F_1N_3O_5$	$C_{35}H_{29}FN_4O_8S$
Crystal system	Monoclinic	Monoclinic	Orthorhombic
Space group	$P2_1/c$	$P2_1/c$	*Pbca*
a (Å)	8.2418	14.1241	8.4541
b (Å)	15.0392	8.8108	18.1835
c (Å)	19.989	21.0359	41.4054
α (deg)	90	90	90
β (deg)	91.61	105.123	90
γ (deg)	90	90	90
V (Å3)	2476.66	2527.15	6365.05
CCDC number	2303274	2303273	2347514

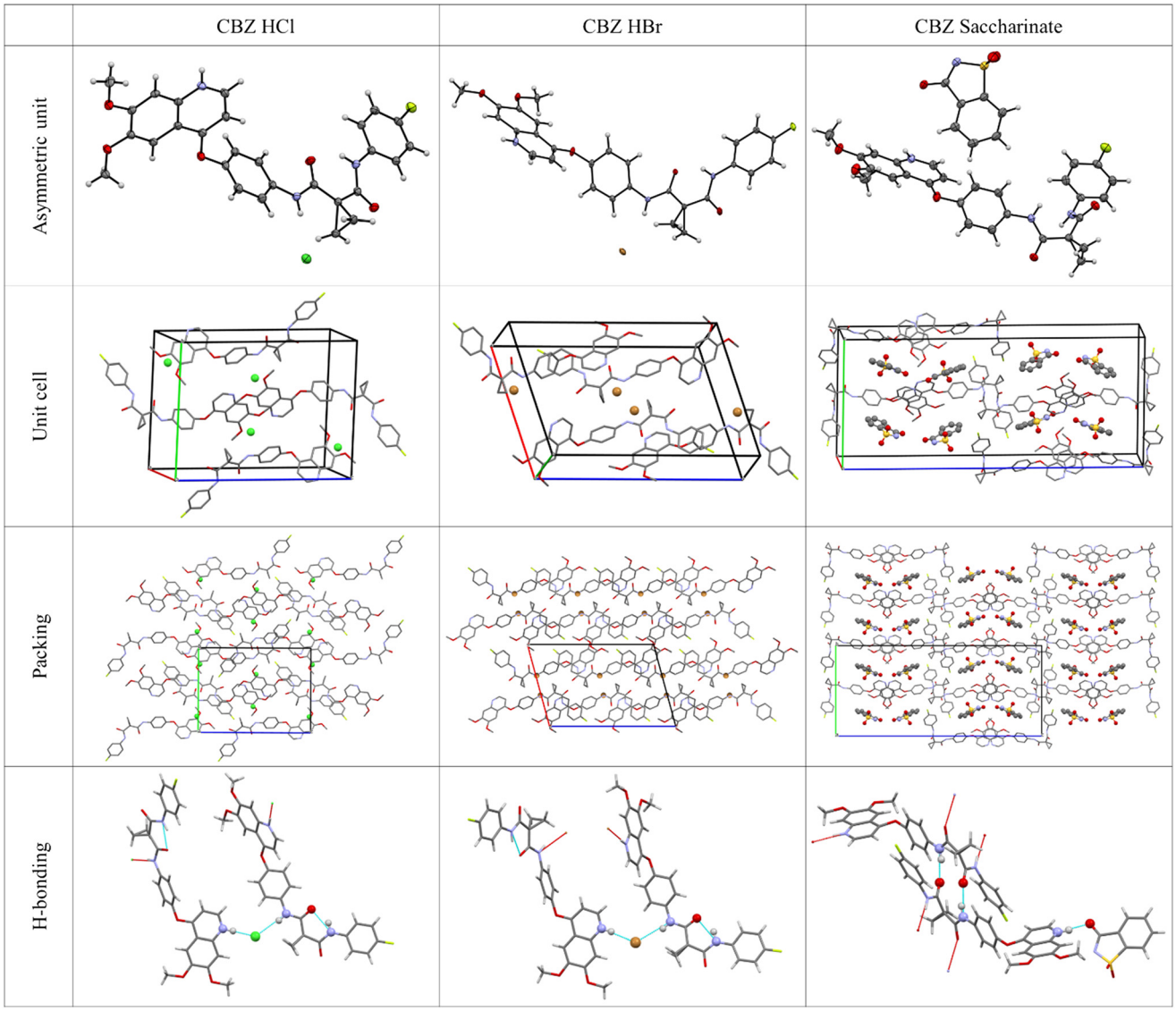

Fig. 3 Crystal structures of CBZ·HCl, CBZ·HBr and CBZ saccharinate salts.

hydrogen bond between the adjacent amidic groups of CBZ N(1)H···O(6). The crystal packing is made possible by the short-range interaction between the oxygen atoms of the methoxy groups and hydrogen atoms on the fluorine-substituted aromatic rings.

CBZ·HBr crystallizes in the monoclinic system in the space group $P2_1/c$. There is one molecule of the CBZ cation and one chloride anion in the asymmetric unit and four of each in the unit cell, thus confirming the 1 : 1 ratio. H-bonding is close to identical as in the CBZ·HCl. The packing in the crystal is made of anti-parallel chains of salt units running both horizontally and vertically.

CBZ saccharinate crystallizes in the orthorhombic system in the space group *Pbca*. There is one molecule of the CBZ cation and one chloride anion in the asymmetric unit and eight of each in the unit cell, thus confirming the 1 : 1 ratio. The main H-bonding pattern is an infinite chain of –CBZ–CBZ– molecules running along the *a* direction connected by ladder-like H-bonds formed by two self-complimentary amidic groups of CBZ, N(18)H···O(25) and N(26)H···O(20). This chain is decorated by hanging saccharinate anions connected by the quinoline N(35)H··· HN(6)amidic H-bonds.

3.4 Thermal analysis and hygroscopicity

In order to confirm the thermal stability and purity of the prepared CBZ·HCl and CBZ·HBr salts, DSC and TGA measurements were performed. DSC thermograms (Fig. 4) of both these salts in our study showed single, sharp melting endotherms, thus confirming the purity of the samples prepared. Their melting points were higher (at least by 40 °C) than the marketed CBZ L-malate salt that had a peak melting temperature of 181.6 °C (Fig. S4†). This observation could be due to the presence of stronger ionic interactions arising from the fact that HCl and HBr are some of the strongest acids known. The high melting points indicate the high

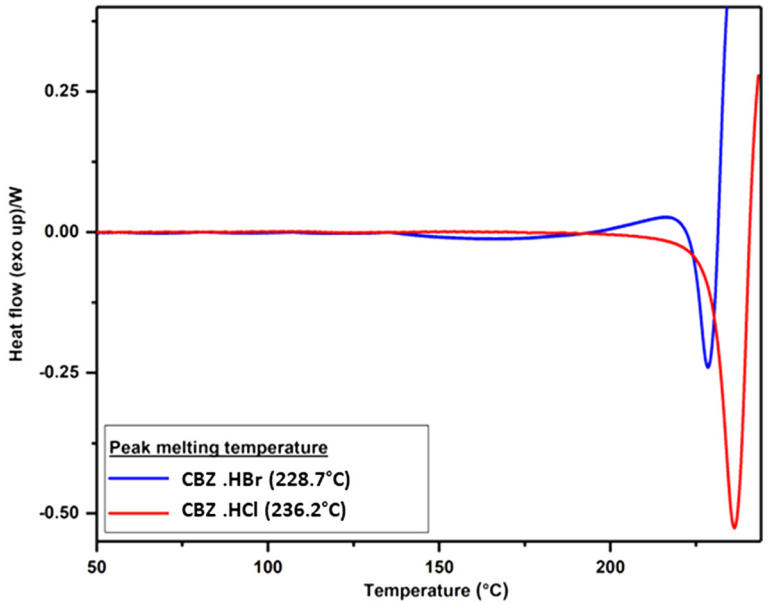

Fig. 4 DSC thermograms of the CBZ·HBr and CBZ·HCl salts.

thermal stability of the salts thereby making them suitable for pharmaceutical development purposes. Furthermore, TGA (Fig. S5†) revealed no significant loss of the sample weight for either salt, confirming that the samples are pure, crystalline, and non-solvated.

Inorganic acids, such as HCl or HBr, are known for their strong polarity, which contributes to the formation of salts that are more susceptible to water uptake.[27] Hygroscopicity is a critical factor in the pharmaceutical industry, as excessive moisture absorption can compromise the physical stability of solid dosage forms during storage. Hence, the hygroscopicity of the CBZ·HBr and CBZ·HCl salts were checked using DVS analysis (section S4†). In both these cases, it was found that there was no significant water uptake, thereby proving their physical stability against humidity.

3.5 Biorelevant dissolution for food effect studies

The change in the dissolution behaviour of the CBZ·HCl and CBZ·HBr salts compared to the marketed form, the CBZ L-malate salt, in the fed and fasted states was predicted by recording intrinsic dissolution rates of these salts in biorelevant dissolution media (FaSSIF and FeSSIF). These media have been found to model the composition of the intestinal contents before and after a meal intake.[28] Dissolution tests conducted in biorelevant media are extensively utilized to predict the *in vivo* behavior of drugs, including their food-effect profiles.[29] Even though the CBZ·HCl salt had the highest dissolution rate in the fasted state (Fig. 5), the variability in the dissolution rates between the fasted and fed states was approximately the same as in the CBZ L-malate salt. While the CBZ L-malate salt showed a 2.5- fold increase in the dissolution rate in FeSSIF compared to FaSSIF (Fig. 5), for the CBZ·HCl salt, the increase was ~3-fold. The CBZ·HBr salt was found to dissolve two times faster than the CBZ L-malate salt in the fasted state (Fig. 5). In FeSSIF, the increase in the dissolution rate for the CBZ·HBr salt was found to be 1.7 times that of the rate in FaSSIF, which suggests persistence of a positive food effect but less variability than the marketed L-malate salt and also the CBZ·HCl salt.

4. Conclusions

In this study, the preparation of five crystalline salts (with hydrochloric acid, hydrobromic acid, cyclamic acid, saccharin, and tartaric acid) of cabozantinib is described. The hydrobromide and hydrochloride salts were chosen for further characterization because their dissolution rates were higher than the marketed L-malate salt compared to the other novel salts. Both these salts displayed higher thermal stability with melting points at least 40 °C higher than the L-malate salt. These salts were found to be non-hygroscopic as well, making them suitable candidates for formulation purposes.

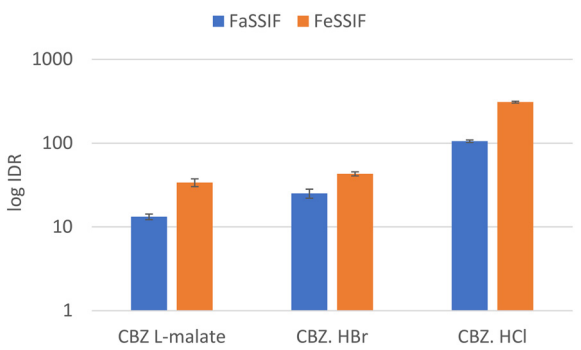

Fig. 5 Log IDR (IDR originally measured in units μg cm^{-2} min) for CBZ L-malate, CBZ·HCl and CBZ·HBr salts in FaSSIF and FeSSIF.

The variability in the dissolution rates of these salts in biorelevant media mimicking the fasted and fed conditions of the human intestine was used to determine the potential of the novel salts to diminish the undesired food effect of the marketed form. Even though the variability between the fed and fasted states was observed for all salts, the hydrobromide salt offers a ~30% improvement over the marketed form of L-malate. The food effect, even though still expected to happen, occurs to a lesser extent than the marketed form when the hydrobromide salt is used. Further *in vivo* studies are required to conclude the potential of these salts to be used in humans.

Data availability

Crystallographic data for the solid forms of cabozantinib (salts of cabozantinib with HCl, HBr and saccharine) have been deposited at the CCDC under 2303274, 2303273 and 2347514 and can be obtained from **https://www.ccdc.cam.ac.uk/structures/?**.

The data supporting this article have been included as part of the ESI.† This contains IR spectra for prepared solid forms, solution ^{1}H NMR spectra, XRPD diffractograms, IDR profiles, DSC signals from the CBZ L-malate salt, TGA curves for CBZ·HBr, CBZ·HCl and CBZ, and DVS curves for CBZ·HCl and CBZ·HBr as well as full crystallographic information about the prepared new solid forms.

Conflicts of interest

There are no conflicts to declare.

Acknowledgements

We would like to acknowledge the Solid-State Department of Zentiva, k.s. for the materials and all the help provided. Our great thanks go to Ondřej Dammer, Lukáš Krejčík, and Marcela Tkadlecova. This work received financial support from the project New Technologies for Translational Research in Pharmaceutical Sciences (NETPHARM), project ID CZ.02.01.01/00/22_008/0004607, co-funded by the European Union, and specific university research grants (A1_FCHI_2022_006, A2_FCHI_2021_016) and by the Czech Science Foundation project 24-10558S. This work was also supported by the CzechNanoLab project LM2018110 funded by MEYS CR, which is gratefully acknowledged for the financial support of the measurements/sample fabrication at the LNSM Research Infrastructure. We would also like to thank the Pharmaceutical Applied Research Center (PARC) for support in various parts of this project.

References

1 C. Y. Wu and L. Z. Benet, *Pharm. Res.*, 2005, **22**, 11–23.
2 K. A. Lentz, *AAPS J.*, 2008, **10**(2), 282–288.
3 **https://www.fda.gov/files/drugs/published/Food-Effect-Bioavailability-and-Fed-Bioequivalence-Studies.pdf** (accessed on 27 November, 2023).
4 F. M. Yakes, J. Chen, J. Tan, K. Yamaguchi, Y. Shi, P. Yu, F. Qian, F. Chu, F. Bentzien, B. Cancilla and J. Orf, *Mol. Cancer Ther.*, 2011, **10**(12), 2298–2308.
5 T. K. Choueiri, B. Escudier, T. Powles, P. N. Mainwaring, B. I. Rini, F. Donskov, H. Hammers, T. E. Hutson, J. L. Lee, K. Peltola and B. J. Roth, *N. Engl. J. Med.*, 2015, **373**(19), 1814–1823.
6 **https://www.accessdata.fda.gov/drugsatfda_docs/label/2012/203756lbl.pdf** (accessed on 27 November, 2023).
7 **https://www.accessdata.fda.gov/drugsatfda_docs/label/2021/208692s010lbl.pdf** (accessed on 27 November, 2023).
8 Cabozantinib s-malate **https://pubchem.ncbi.nlm.nih.gov/compound/Cabozantinib-S-malate** (accessed on 27 November, 2023).
9 L. Nguyen, J. Holland, R. Mamelok, M. K. Laberge, J. Grenier, D. Swearingen, D. Armas and S. Lacy, *J. Clin. Pharmacol.*, 2015, **55**(11), 1293–1302.
10 M. Herbrink, B. Nuijen, J. H. Schellens and J. H. Beijnen, *Cancer Treat. Rev.*, 2015, **41**(5), 412–422.
11 M. Veerman, K. Hussaarts, F. Jansman, S. Koolen, R. Leeuwen and R. Mathijssen, *Lancet Oncol.*, 2020, **21**(5), e265–e279.
12 R. Z. Szmulewitz and M. J. Ratain, *Clin. Pharmacol. Ther.*, 2013, **93**(3), 242–244.
13 H. D. Williams, L. Ford, S. Han, K. J. Tangso, S. Lim, D. M. Shackleford, D. T. Vodak, H. Benameur, C. W. Pouton, P. J. Scammells and C. J. Porter, *Mol. Pharmaceutics*, 2018, **15**(12), 5678–5696.
14 S. M. Berge, L. D. Bighley and D. C. Monkhouse, *J. Pharm. Sci.*, 1977, **66**, 1–19.
15 E. Skorepová, D. Bím, M. Hušák, J. Klimes, A. Chatziadi, L. Ridvan, T. Boleslavská, J. Beránek, P. Šebek and L. Rulísek, *Cryst. Growth Des.*, 2017, **17**, 5283–5294.
16 S. Ramesh, E. Skořepová, V. Eigner, V. C. Paingad, V. Zvoníček, P. Kužel and M. ŠóóŠ, *Cryst. Growth Des.*, 2022, **23**(1), 168–179.
17 K. C. Mannava, K. Suresh and A. Nangia, *Cryst. Growth Des.*, 2016, **16**, 1591–1598.
18 **https://go.drugbank.com/drugs/DB08875** (accessed on 27 November 2023).
19 S. L. Childs, G. P. Stahly and A. Park, *Mol. Pharmaceutics*, 2007, **4**, 323–338.
20 B. Kapadiya Dhartiben and K. D. Aparnathi, *Int. J. Curr. Microbiol. Appl. Sci.*, 2017, **6**(6), 1283–1296.
21 Tartaric acid **https://go.drugbank.com/drugs/DB09459** (accessed on 1 December, 2023).
22 T. Munegumi, *World J. Chem. Educ.*, 2013, **1**(1), 12–16.
23 *CrysAlisPRO*, Oxford Diffraction/Agilent Technologies UK Ltd, Yarnton, England.
24 V. Petříček, M. Dušek and L. Palatinus, *Z. Kristallogr. - Cryst. Mater.*, 2014, **229**, 345–352.
25 L. Palatinus and G. Chapuis, *J. Appl. Crystallogr.*, 2007, **40**, 786–790.
26 J. Rohlíček and M. Hušák, *J. Appl. Crystallogr.*, 2007, **40**, 600–601.

27 D. Gupta, D. Bhatia, V. Dave, V. Sutariya and S. Varghese Gupta, *Molecules*, 2018, **23**(7), 1719.
28 J. B. Dressman and C. Reppas, *Eur. J. Pharm. Sci.*, 2000, **11**, S73–S80.
29 S. Klein, *AAPS J.*, 2010, **12**(3), 397–406.